Briongos, J. V., Gómez-Hernández, J., González-Gómez, P. A. & Serrano, D. (2018). Two-phase heat transfer model of a beam-down gas-solid fluidized bed solar particle receiver. *Solar Energy*, 171, pp. 740–750.

DOI: 10.1016/j.solener.2018.07.016

Two-phase heat transfer model of a beam-down gas-solid fluidized bed solar particle receiver

*Briongos, J.V., Gómez-Hernández, J., González-Gómez, P.A., Serrano, D.

Universidad Carlos III de Madrid. Escuela Politécnica Superior. Departamento de Ingeniería Térmica y de Fluidos, Avenida de la Universidad 30, 28911, Leganés (Madrid)
*Correspondence to the author, e-mail: jvilla@ing.uc3m.es

Abstract:

Beam-down concentrating solar power for thermochemical and energy absorption applications stands as an attractive approach that can enhance the renewable energies deployment. This work explores the integration of beam-down optics with fluidized bed technology proposing a model to calculate both gas and bed temperatures. The beam-down system concentrates the energy from the solar field into a fluidized bed receiver. A novel phenomenological model is proposed to adapt the well-known two-phase theory to the heat transfer process of a bed operating in the bubbling regime while it is directly irradiated from the top. In this way, this simple model can be used as a design tool for beam-down fluidized bed receivers. The top bed surface is considered as an opaque diffuse layer formed by gray particles. A single layer model is applied to estimate the effective emissivity between the heterogeneous bed surface and the ambient conditions in the freeboard. The vertical temperature profile is obtained considering particle phase heat conduction, particle to gas heat convection, solid convection, bubble convection and radiation heat transfer mechanisms. The model is validated using silicon carbide and zirconia fluidized bed experiments reported in the literature. The model shows that the solid convection is the dominant heat transfer mechanism for a beam-down fluidized bed receiver. Further results explore the influence of the operating conditions on the fluidized bed receiver for a bed of silicon carbide particles, showing that energy concentration fluxes of $35 \cdot 10^4$ W/m^2 can reach bed temperatures of 1000ºC when operating at a gas velocities of $3 \cdot U_{mf}$.

Keywords:

concentrating solar power; beam-down optics; solar particle receiver; fluidized beds heat transfer; two-phase model

1. Introduction.

Renewable energy deployment should be the sustainable response of the industry and the scientific community to meet the growing energy requirements of our society. Among renewable technologies, wind and solar systems have shown its feasibility to replace conventional non-renewable technologies in many commercial applications. The integration of concentrating solar power (CSP) systems with thermal storage is one of the most promising technologies due to its high dispatchability (Siegel et al., 2013,Tregambi et al., 2017). This technology enhances also the possibility of managing heat generation on a local level for thermochemical processes such as calcium looping (Siegel et al., 2013,Tregambi et al., 2017,Ortiz et al., 2017,Alovisio et al., 2017).

In this line, the concentration of sunlight on particle-based receivers appears as an interesting technology for such applications due to the use of solid particles as the heat transfer medium, which can reach high temperatures (~1000ºC). Recent concepts of central particle receivers have been reviewed in (Ho, 2016), showing four main types of direct particle heating receivers: free-falling, obstructed flow, rotating kiln/centrifugal and fluidized particle receivers. In these systems, the particle receiver is located on the top of a central tower, where all heliostats concentrate the sunlight.

However, it is possible to substitute the tower by a secondary reflector system, redirecting the concentrated solar energy to a ground receiver. In this way, the energy of all heliostats is focused to a beam-down reflector, where the radiation is redirected to the top of a particle receiver reaching high energy concentrations (Segal and Epstein, 2000). This heliostats configuration eases the operation and maintenance of the ground reactor and reduces the costs of the tower and the heat transport system (Yadav and Banerjee, 2016). The beam-down disadvantages are the costs associated to the construction of the secondary reflector and the large magnification at the ground receiver (Vant-Hull, 2013). Therefore, a cost-benefit analysis should be considered for each process. Examples of the beam-down reflector coupled with a fluidized bed receiver have shown its usefulness (Calvet et al., 2016,Kodama et al., 2010). Another beam-down approach has been recently presented in (Gómez-Hernández et al., 2017) where, instead of focusing on a single point, the beam-down reflector concentrates linearly on the particle receiver while the solids are moving horizontally. Therefore, the beam-down with a ground receiver approach enhances the application of fluidized bed technology to thermochemical processes (Segal and Epstein, 1997,Segal and Epstein, 2003,Kodama et al., 2010,Gokon et al., 2012), or energy capture processes (Calvet et al., 2016,Kodama et al., 2013,Kodama et al., 2017).

Gas-solid fluidized beds are used in many industrial applications due to their heterogeneous medium, which is characterized by high heat transfer rates and high energy densities. Many efforts have been made to analyze the complex hydrodynamic behavior of the dense gas-solid flow in these reactors. Numerical models, such as Eulerian-Eulerian or Eulerian-Lagrangian, together with computational fluid dynamics (CFD) and discrete element method (DEM) models have been developed to obtain accurate flow characteristics (Van Wachem et al., 2001,Bellan et al., 2018). Analogously, the heat transfer process between the gas and the particles has been carefully analyzed such as in conventional fluidized bed dryers, gasifiers or combustors (Davidson et al., 1985,Chen et al., 2005,Molerus, 1997a,Chen and Chen, 1981,Tien, 1988). However, in contrast to traditional fluidized bed heat transfer processes, beam-down fluidized bed receivers collect the energy at the top layer of particles and therefore, the question about how this thermal energy is transferred through the bed is still open. To solve that, the particle phase heat conduction, particle to gas heat convection, solid convection, bubble convection and radiation heat transfer mechanisms should be considered. Furthermore, the complex nature of

the gas-solid flow makes the modeling of these heat transfer processes not straightforward. To the best author knowledge, only (Flamant, 1982), which determined the penetration of the radiation in a fluidized bed, and (Tregambi et al., 2016), which studied the solids circulation parameter in a fluidized bed at different gas velocities, have analyzed the heat transfer processes for beam-down optics coupled to fluidized beds. Here, a classical approach is proposed to describe the heat transfer of a fluidized bed that directly receives the radiation to the bed surface.

In this work, a theoretical transient model is proposed to describe the heat transfer process of a directly irradiated gas-solid bubbling fluidized bed. The proposed model provides clear information to guide design and operation of beam-down irradiated particle receivers, as it takes into account the hydrodynamic behavior of the bed when solving the heat transfer problem. The model is based on the well-known two-phase theory of fluidization as it is simpler and with lower computational costs than other numerical models. The validation of the model is carried out using data previously reported by (Flamant, 1982) for silicon carbide and zirconia particles. Once the model is validated, its performance is studied simulating a bed of silicon carbide particles and air as fluidizing gas in order to determine the feasibility of the beam-down fluidized bed system. The results show how the operating conditions can change the temperature profiles of both fluidizing gas and particles. The case study shows the usefulness and clarity of the proposed model to better understand the heat transfer processes in these receivers and optimize its design and operating conditions.

2. Beam-down fluidized bed receiver and simulation conditions

Figure 1-A illustrates the operational concept of the whole system. The layout of the receiver is composed by a field of heliostats that reflects the sunlight aiming to a secondary reflector. This beam-down optical system, which can be constructed following an ellipsoid or a hyperboloid mirror (Segal and Epstein, 2000), concentrates the radiation on the top of the ground receiver. The ground receiver consists on a fluidized bed that receives the concentrated radiation from the top. The direct irradiation on the bed creates a layer of hot particles on the bed surface. According to the proposed model, as the fluidized bed is operated at bubbling conditions to promote a high gas-solid mixing and a high heat transfer rate, the hot layer will be moved to the bottom of the bed due to the solid convection driven by the flow of rising bubbles. This transient process reaches the equilibrium state when the energy captured by the particles is balanced with the energy transferred to the fluidizing gas. Figure 1-B shows the temperature profile of the bed particles at the steady state identifying three zones: (1) top surface where the energy is focused, (2) bulk bed zone characterized by the degree of mixing between gas and particles, and (3) the bed bottom region near the distributor.

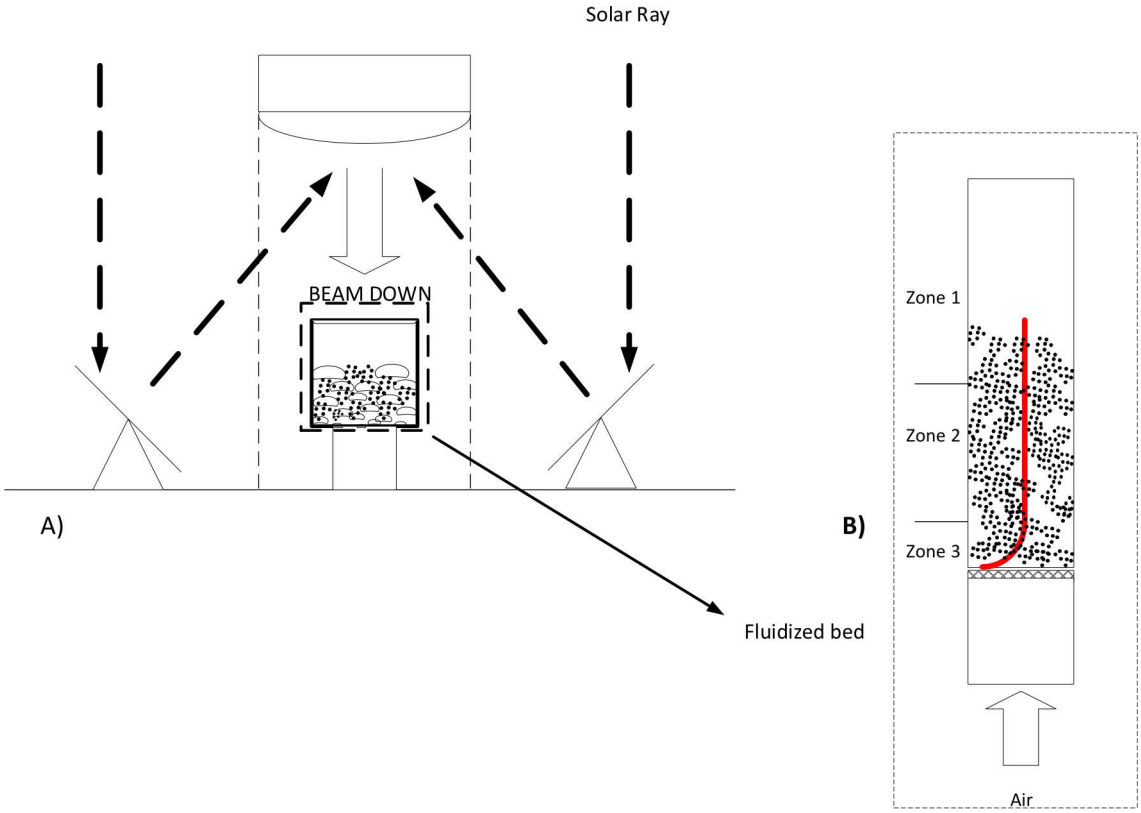

Figure 1. Schematic diagram of the particle receiver: (A) Layout of a beam-down optic system and the fluidized bed receiver; (B) particle temperature profile within the bed.

Three sets of simulations have been carried out in order to: (i) validate the model, (ii) check the influence of the operating conditions on the bed performance, and (iii) characterize the transient response of the model. First, the results of (Flamant, 1982) are reproduced analyzing a bed of 0.065 m of internal diameter (*ID*), porous plate distributor, and static bed height of 0.1 m high for different relative gas velocities, $U_r = U_0/U_{mf}$, and energy flux densities, $\emptyset_{in}$. Silicon carbide and zirconia particles are simulated separately, their properties at high temperatures are shown in Table 1 (Incropera et al., 2013,Modest, 2013,Geldart, 1986,Verein, 2010). The emissivity data provided in (Mullinger and Jenkins, 2008) is used to consider the temperature effect on the particle emissivity during the simulations. Following the experiments reported in (Flamant, 1982), air enters at 20ºC to a bed initially at 20ºC.

The second set of tests analyzes the performance of the model simulating a fluidized bed of sand particles air. This receiver is studied for *ID* = 0.6 m, different bed heights and different superficial gas velocities using a perforated plate distributor with ratio of pressure drop to bed pressure drop of $\Delta P_{dist}/\Delta P_{bed}$ = 0.365. Finally, the analysis of the inlet air temperature influence is used as a guide design application for a constant energy flux of $\phi_{in} = 35 \cdot 10^4 W/m^2$.

The third tests study the open loop response of the system analyzing its transient behavior. The characteristic times of each zone (Fig. 1) are computed. The air properties have been calculated with the open-source thermophysical property library CoolProp (Bell et al., 2014).

Table 1. Particle properties.

Material	Particle density, ρ_s [kg/m^3]	Particle sieving diameter, d_p [μm]	Minimum fluidization velocity, U_{mf} [m/s]	Particle conductivity, k_s [W/mK]	Particle specific heat, c_p [J/kgK]	Particle emissivity, ε_p [-]
SiC	3080	250	0.072	16.7	1100	0.82-0.85
ZrO_2	5671	250	0.13	1.44	773	0.36-0.77

3. Two-phase model for directly irradiated beam-down fluidized beds

It is well known that nonlinear dynamics that characterize gas-solid fluidized beds have been a challenge for decades to fluidization engineers. Accordingly, a big research effort has been addressed to understand such nonlinearities (Johnsson et al., 2000,Daw et al., 1990,Briongos et al., 2007,Bokkers et al., 2006,Briongos et al., 2013) in order to develop new models to guide the design and operation of these systems (Bokkers et al., 2006,Briongos et al., 2013,Van Wachem et al., 2001). In this work, a classical approach, such as the two-phase fluidized bed reactors model, is proposed to describe the heat transfer process in a directly irradiated fluidized bed receiver, where the radiation is concentrated uniformly on the top bed surface.

When developing a two-phase model, the relevant physical or dynamical features of the nonlinear behavior of fluidized beds are conceptually arranged in two or three phases (Davidson et al., 1985). These phases might include the gas phase, the solid phase or both gas and solids. According to this model, the bubble voids and the gas through-flow constitute the bubble-phase, whereas the interstitial gas and net flux of interstitial voids moving with the particle flow are considered within the dense-phase. Moreover, it is assumed that all the airflow in excess above minimum fluidization conditions will flow throughout the bed within the visible bubble phase.

The proposed two-phase model for directly irradiated beam-down fluidized beds, takes into account the emulsion phase and the bubble phase. The emulsion phase includes both the solid and the interstitial gas and consequently, is treated as a porous media. The bubble phase includes the gas that passes across the bed as visible bubble flow. According to that, it is assumed that the bubbles are surrounded by large overlapping clouds that may comprise the complete emulsion phase (Kunii and Levenspiel, 1991), Figure 2.

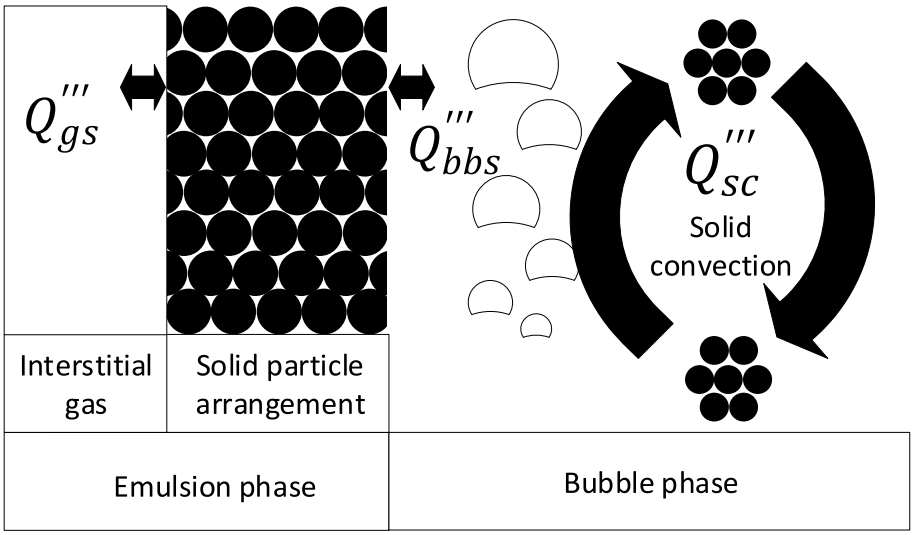

Figure 2. Schematic diagram of the proposed two-phase model where all the solids are assigned to the dense phase.

The first law of thermodynamics is applied to both the emulsion phase (porous medium) and the bubble phase.

- Emulsion phase (porous media):

  Solid phase:

$$(1-a_B)(1-\varepsilon_e)\rho_s c_{ps}\frac{\partial T_s}{\partial t} = (1-a_B)(1-\varepsilon_e)k_e\frac{\partial^2 T_s}{\partial z^2} + (1-a_B)(1-\varepsilon_e)k_r\frac{\partial^2 T_s}{\partial z^2} + Q'''_{sc} + Q'''_{gs} + Q'''_{bbs} \quad (1)$$

  Gas phase:

$$(1-a_B)\varepsilon_e\rho_g c_{pg}\frac{\partial T_{ge}}{\partial t} + U_{ge}\rho_g c_{pg}\frac{\partial T_{ge}}{\partial z} = Q'''_{gs} \quad (2)$$

- Bubble phase:

$$a_B\rho_g c_{pg}\frac{\partial T_{ge}}{\partial t} + U_b\rho_{gb}c_{pgb}\frac{\partial T_{gb}}{\partial z} = Q'''_{bbs} \quad (3)$$

Q'''_{sc} accounts for the heat transferred by solid convection due to the solid circulation inside the bed driven by bubble dynamics, Q'''_{gs} is the term of the particle interstitial gas heat transfer and Q'''_{bbs} refers to the heat transferred between the bubble gas and the emulsion particles.

The equations 1-3 are solved with the following assumptions:

1. The fluidized bed operates at the bubbling regime.
2. Bubble phase is completely free of particles for heat transfer analysis.
3. Bubbles are assumed to be the driver of the fluidized bed dynamics (Briongos et al., 2007) and force the solid convection.
4. Clouds are included within the emulsion phase.
5. The hydrodynamic two-phase theory (Grace and Clift, 1974,Lockett et al., 1967) is used to compute the visible bubble flow that crosses the bed as bubbles. According to that, the flow in the dense bed equals $U_{mf}A_{bed}$, whereas the total flow in the bubble phase equals $(U_0 - U_{mf})A_{bed}$.
6. Concentrated radiation is uniformly distributed on the top surface of the bed.
7. One-dimensional evolutions of both the bubble temperature and the emulsion phase temperature are solved. No axial dispersion is considered either in the dense bed phase or in the bubble phase.
8. Bubble size is calculated according to Mori and Wen model for porous plate and perforate plate distributors (Darton et al., 1977,Mori and Wen, 1975).
9. For continuity consideration regarding energy balance, the absolute bubble velocity as defined in (Davidson and Harrison, 1963) is used.
10. The fluidized vessel is considered to be perfectly insulated.

Furthermore, the constant time-step size used during the simulation runs is fixed to $4\cdot10^{-4}$s, whereas the spatial discretization step equals to $1/(1 - \varepsilon_0)$. The following sections provide information to better understand the proposed model and the different mechanisms involved on it.

3.1. Temperature and pressure effects on gas-solid fluidization dynamics

Fluidized bed behavior is sensitive to both gas density and gas viscosity because of the temperature and pressure conditions. Their effects on the dynamics of gas-solid fluidized beds have been previously reported in literature (Yates, 1996,Shabanian and Chaouki,

2017,Knowlton, 1999). As the change in the gas properties modifies the gas-particle forces, the variations of the local superficial gas velocity influence the bubble dynamics changing the circulation pattern of solids. Thus, it is necessary to consider both pressure and temperature effects depending on the Geldart's classification of the particles (Geldart, 1973,Geldart and Abrahamsen, 1978,Molerus, 1982). For powders of B or D type-like groups, most of the correlations reported in the literature are able to predict the behavior for high temperature and high-pressure conditions (Shabanian and Chaouki, 2017). However, the influence of the gas pressure on the bubble dynamics is only significant above 25 bar, which is far from the operating conditions considered here. Thus, in this work, in which B-group particles are studied, only the influence of the temperature is considered regarding to bubble dynamics and no effect of the pressure is taken into account.

3.2. Heat transfer in gas-solid fluidized beds

Fluidized beds provide a large area of contact between the particles and the fluidizing gas, which increases the heat transfer rates between both the solid and the gas phases (Kunii and Levenspiel, 1991). The high degree of solid mixing due to bubbling decreases the appearance of temperature gradients through the bulk of the bed and gives rise to a high effective internal thermal conductivity. In this sense, the solids convection is critical for the beam-down fluidized bed receiver considered in this work. The understanding of the heat transfer mechanisms is critical for a proper design and an optimum operation. According to that, the particulate phase heat conduction, particle to gas heat convection, and radiation heat transfer are considered to model the heat transport phenomena in a gas-solid fluidized bed solar receiver directly irradiated from the top.

3.2.1. Heat transfer by conduction mechanism

According to the literature, it is generally accepted that the effective conductivity, k_e, might be obtained by the contribution of two components in order to take into account both the effect of the turbulent diffusion and the fixed bed conductivity (Davidson et al., 1985). However, in a beam-down fluidized bed receiver, the radiant solar flux concentrated by the beam-down optical system is absorbed at the top surface of the bed, and therefore, the heat transfer process takes place in opposite direction of the gas flow. Therefore, it is assumed that turbulent diffusion will not increase the effective conductivity of the bed and, as a consequence, the fixed bed motionless fluid conductivity, k_e^0, is used to account for the particle-particle conduction heat transfer.

$$k_e^0 = k_g \cdot \left(\frac{k_s}{k_g}\right)^{\left[0.28-0.757\log_{10}\varepsilon_0-0.057\log_{10}\left(k_s/k_g\right)\right]} \quad (4)$$

3.2.1. Heat transfer by convection mechanism

The thermal energy transferred by convection is analyzed as the sum of three contributions: the particle to gas heat transfer through the emulsion phase, the heat transferred between the emulsion phase and the gas of the bubble phase, and the heat transferred along bed by means of solid convection.

Most applications of bubbling fluidized beds involve the heat transfer between the fluidized bed and immersed surfaces (Chen et al., 2005). However, in beam-down fluidized bed receiver applications, the particle to gas heat transfer is the main mechanism to transfer thermal energy to the fluidizing gas. There are different correlations reported in literature to estimate the heat transfer coefficient, here the empirical expression described in (Kunii and Levenspiel, 1991) is used:

$$h_{gp} = \left(\frac{k_g}{d_p}\right) 0.03 Re_p^{1.3} \quad (5)$$

As stated above, the proposed model differentiates between the particle to gas heat transfer that takes place along the emulsion phase, which is calculated by Eq. 5, and the heat transfer between the bubble gas and the dense bed. It is worth to point out that Eq. 6 does not consider the heat transfer from or to particles in the bubble phase assuming thin clouds, and therefore, it is established that all the particles are associated with the dense phase from a convection heat transfer point of view:

$$h_{bc} = 0.975 \rho_g c_{pg} \left(\frac{k_g}{\rho_g c_{pg}}\right)^{1/2} \left(\frac{g}{d_B}\right)^{1/4} \quad (6)$$

The heat transferred by solids circulation that takes place in the bulk phase, due to bubble driven dynamics, is the result of the energy balance between the upward and the downward flux of solid in the bed:

$$w(1 - a_{BW}) = U_b f_w a_{BW} \quad (7)$$

Where *w* is the circulation rate as defined in (Davidson et al., 1985).

Finally, a gas heating thermal efficiency, η_g, can be defined as the ratio between the heat transferred from solids to gas and the energy flux incident on the particle receiver (Flamant and Olalde, 1983), Eq. (8).

$$\eta_g = \frac{\text{Power transferred to the heat transfer fluid}}{Incident\ power} \quad (8)$$

3.2.3. Heat transfer by radiation mechanism

It is widely accepted in literature that the radiation heat transfer mechanism should be considered for bubbling beds operating at temperatures greater than 500ºC (Flamant et al., 1992,Chen et al., 2005,Geldart, 1986). However, when the particle convection is important, heat transfer by radiation inside de bed is not the major heat transfer mechanism even at high temperatures (Molerus, 1997b). As observed below, the bed medium is considered opaque and diffuse, and consequently, it is considered optically thick within the emulsion phase. Such approach has been previously used in the literature in the framework of the two-phase model (Strieder, 1997,Chen and Chen, 1981,Flamant and Olalde, 1983). In this work, the thick approximation is used following the diffusion approximation (Modest, 2013). Accordingly, the radiative heat flux for an isotropically gray scattering medium can be reduced to the so-called Rosseland approximation:

$$q_r = -k_r \frac{\partial T}{\partial z} \quad (9)$$

Where the radiative conductivity is given by:

$$k_r = \frac{16n^2\sigma T_s^3}{3\beta_R} \quad (10)$$

In order to calculate the Rosseland mean extinction coefficient, β_R, shown in Eq. 10, it is assumed that the emulsion is formed by a monodispersed spherical particles following the approach reported in (Tien, 1988). Thus, the absorption coefficient is given as:

$$\beta_R = \frac{3Q_a f_v / d_P}{2} \quad (11)$$

The extinction coefficient values provided by Eq. 11 are of the same order of magnitude than the extinction coefficient reported in (Flamant, 1982).

The top bed surface is treated as an opaque diffuse layer formed by gray particles to model the heat transfer by radiation. The effective isothermal bed absorptivity, α_{bed}, for the upper layer is calculated according to (Mazza et al., 1991) in order to consider the energy absorbed by the particles from the total energy flux incident on the receptor surface. This effective bed absorptivity is larger than the particle absorptivity due to the cavity effect of the heterogeneous bed surface, which is affected by the particle scattering in the bed surface.

Regarding the energy leaving the bed surface by radiation, a double particle layer model is applied to estimate the effective emissivity of the heterogeneous bed surface (Modest, 2013) . This effective bed surface emissivity, $\varepsilon_{eff} = \varepsilon_p F_{b-a}$, is computed as the product between the particle emissivity and the vision factor from the top surface particles to the surrounding ambient air in the freeboard. Figure 3 depicts how the vision factor (F_{b-a}) between the top surface particles and the ambient air is calculated. The value of the vision factor obtained for a single particle layer is computed using the view factor relations detailed in the Appendix, and is composed by two terms taking into account both the tangent direction and the normal direction (Fig. 3-b/c). The view factor estimated through this approach is similar to the results obtained for a double particle layer model reported previously by (Gao et al., 2002) to model the heat transfer between a fluidized bed and an immersed surface.

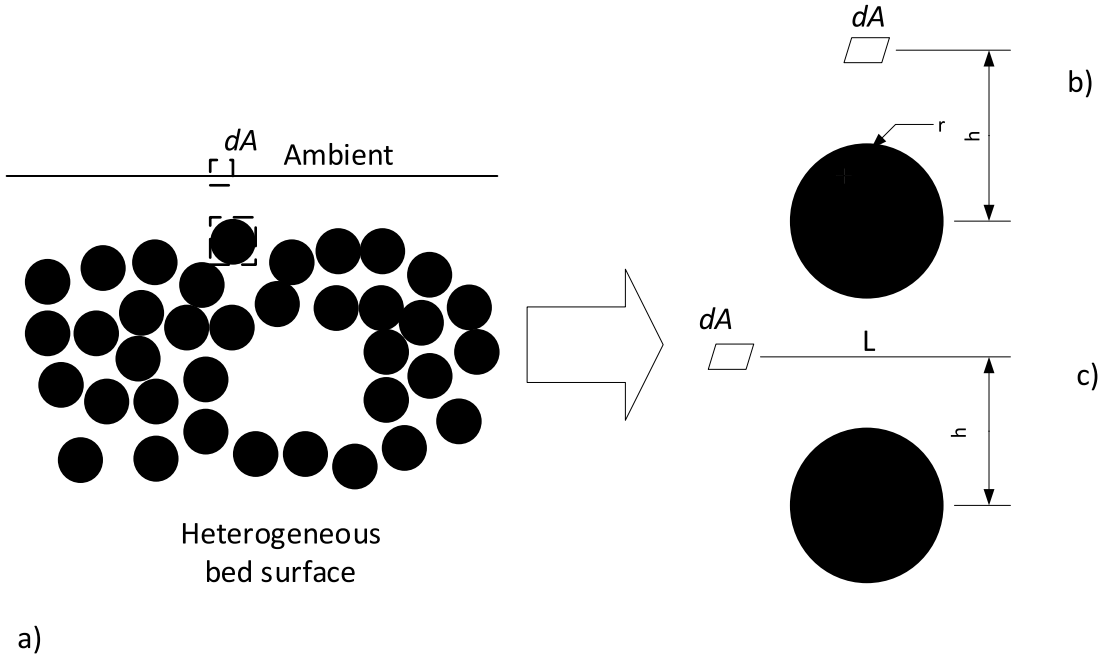

Figure 3. Radiation mechanism on the bed surface. a) Heterogeneous bed surface; b) vision factor between a planar element and a sphere in normal direction, adapted from (Modest, 2013);

c) vision factor between a planar element and a sphere in tangent direction, adapted from (Modest, 2013).

Finally, the geometric effect of the vessel outlet is considered including the conventional vision factor for coaxial parallel disks, F_{ij} (Modest, 2013).

3.2.4. Boundary conditions.

For simplicity, the temperature of the fluidizing air and the emulsion phase at the bottom are assumed to be in thermodynamic equilibrium and therefore, the emulsion phase temperature at that point equals the inlet air temperature. In contrast, the boundary condition at the top bed surface is calculated using the following energy balance:

$$Q'''_{net} = Q'''_{in} - Q'''_{out} \quad (12)$$

$$Q'''_{net} = \emptyset_{in,a_p} a_p - \left(Q'''_{r,out} + Q'''_{conv,loss} + Q'''_{air,out}\right) \quad (13)$$

Where the thermal energy gained or lost by the bed surface is the difference between the energy received from the beam down input, Q_{in}, and the energy output, Q_{out}. a_p takes into account the specific surface of particles at the top of the bed. Thus, the total energy flux absorbed at the bed surface, $\emptyset_{in,a_p}$, reads as:

$$\emptyset_{in,a_p} = \alpha_{bed} \emptyset_{in} \frac{A_{bed}}{A_{p,sL}} \quad (14)$$

Where $A_{p,sL}$ is the effective heat transfer area at the top bed considering all particles fluidizing at the bed surface. The convection losses, $Q_{conv\,loss}$, consider the convective heat transfer at the surface to the corresponding emulsion phase, bubble phase and solid convection. The air loss term, $Q_{air,out}$, reflects the energy gained by the fluidizing air through the bed.

$$Q_{air,out} = \dot{m}_{air} c_{p,air} \left(T_{air,out} - T_{air,in}\right) \quad (15)$$

Finally, the radiative heat loss term, $Q_{r,out}$, is calculated from an energy balance on the bed surface. Thus, in agreement to the thick medium approach used within the bed, the top bed surface is treated as an opaque diffuse and gray surface. Furthermore, the bed surface radiative heat losses are considered using an sky effective temperature of $T_{sky} = 293\ K$:

$$Q'''_{r,out} = \varepsilon_{eff} \sigma F_{ij} a_p \left(T^4_{bed,s} - T^4_{sky,}\right) \quad (16)$$

4. Results and discussion

This section first presents the validation results comparing experimental (Flamant, 1982) and simulation outputs for SiC and ZrO_2 beds of *ID* = 0.065 m and static bed height of *H* = 0.1 m. Then, the influence of the operating conditions on the model results is analyzed for a silicon carbide bed of *ID* = 0.6 m. In these sections, the temperature results are shown for steady-state conditions. Finally, the transient response of the model is studied to determine the characteristic time of each bed zone.

4.1. Model validation.

Figure 4 shows the comparison of the model temperature profiles and the experimental data reported in (Flamant, 1982) for a bed of silicon carbide with 0.10 m static bed height (Table 1). Constant energy flux of ϕ_{in} = 20·10^4 W/m^2 and relative gas velocities of U_r = 1.3, 1.5, and 1.7 are set to measure the temperature at different heights for steady state conditions. The symbols identify the experimental results obtained in (Flamant, 1982) while the lines represent the predicted temperatures provided by the proposed model.

There is a good agreement between the experimental data and the simulated data predicted by the proposed model. The model results show similar trends to the experimental results, identifying the three zones that characterize the bed receiver and its size. However, the temperature predictions deviate from the experimental measurements in zone 3, near the distributor plate. This effect is produced by the tight boundary condition imposed at the distributor plate, which implies that at the bed bottom the temperature of the emulsion phase equals the air inlet temperature.

Regarding zone 2, it is worth to point out that there are no temperature gradients since the solid convection is high enough to guarantee uniform temperatures. Furthermore, it can be observed that the bulk bed temperature decreases as increasing the gas velocity and consequently, the size of region 2 increases. Other result shown from Fig. 2 is that the vertical temperature distribution decreases as increasing air mass flow due to the bed to air convection heat transfer.

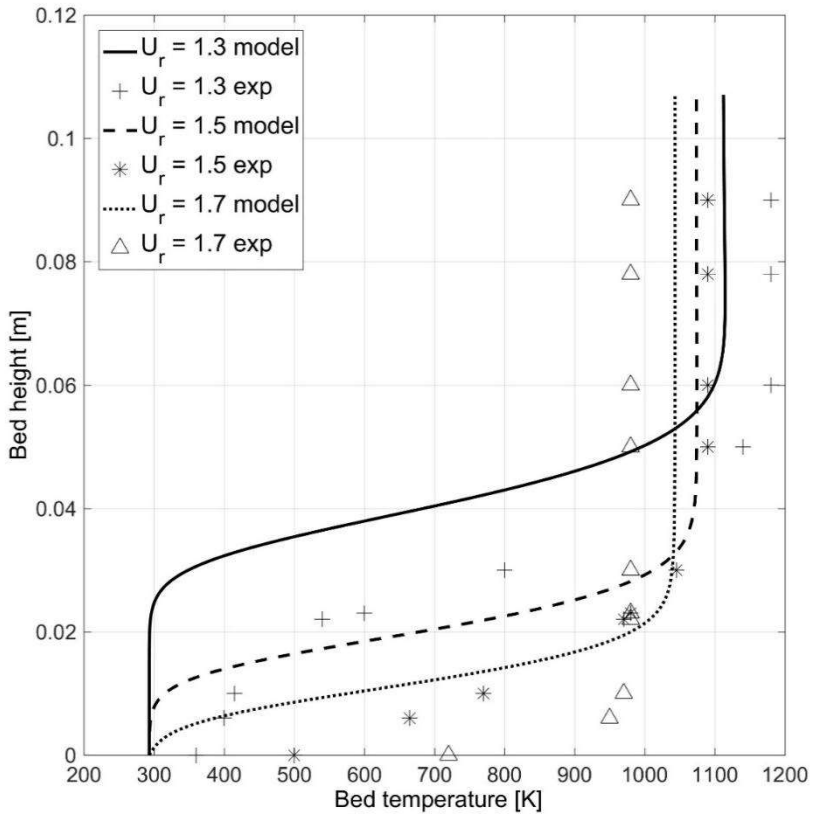

Figure 4. Vertical temperature distribution in a fluidized bed of *ID* = 0.065 m with silicon carbide particles ($\emptyset_{in}$ = 20·10^4 W/m^2, $T_{air,in}$ = 20ºC). "Exp" refers to experimental results reported in (Flamant, 1982).

The influence of the heat energy flux on the equilibrium temperature for zirconia and silicon carbide fluidized beds is shown in Figure 5. Experimental results are plotted in solid lines (SiC)

and dashed lines (ZrO_2), which are obtained for a relative gas velocity in a range of $1.5 < U_r < 1.7$ (Flamant, 1982), while the model results are plotted in symbols. The observed bed temperatures follow a roughly linear trend when increasing the mean flux density. This behavior is fairly well reproduced by the model. It can be observed that the model almost matches the temperatures for silicon carbide particles, only a small deviation is observed for the lowest energy fluxes of $23 \cdot 10^4$ W/m^2. In contrast, zirconia bed temperatures show less agreement to the experimental data reported in (Flamant, 1982). In this case, this disagreement can be produced by the different properties of ZrO_2 particles used in (Flamant, 1982) and the properties used in the model that were found in the literature. As was found in the literature, ZrO_2 properties depend on its composition and thermal treatment, which could be different to (Flamant, 1982). On the contrary, silicon carbide properties are well known in the literature, explaining the good match between our model and the experimental results.

Therefore, according to the results shown in Fig. 5, the use of reliable particle properties becomes a critical aspect to model fluidized beds operating at these high temperature conditions. Nevertheless, the close match between the model and the reported data makes the proposed model a promising tool for designing and operation optimization.

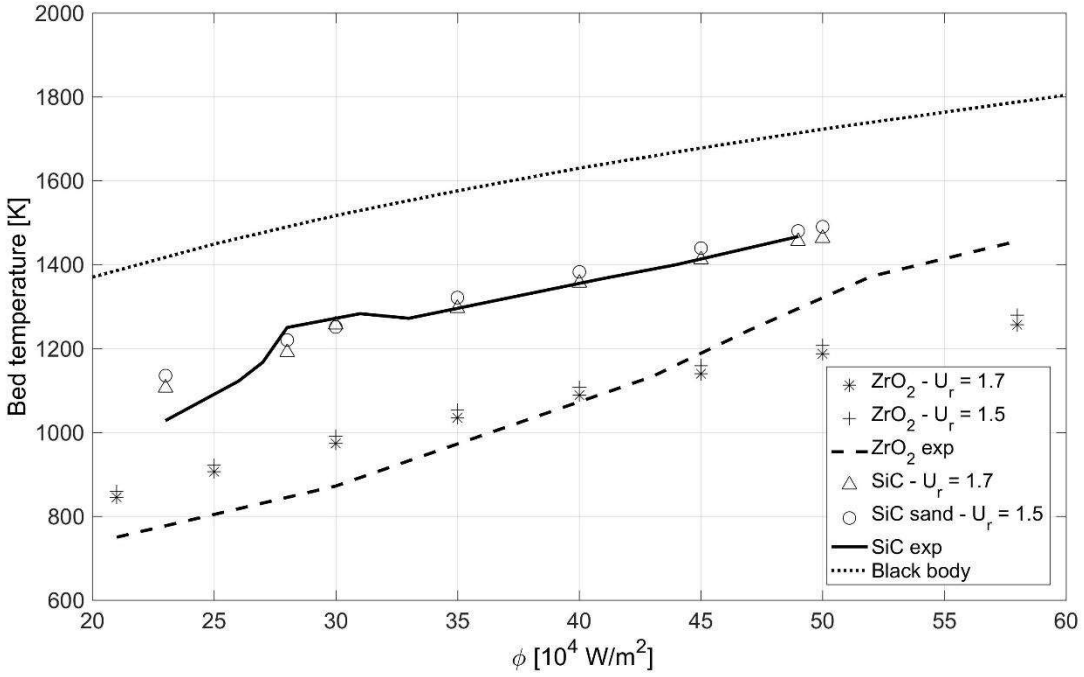

Figure 5. Equilibrium temperature of the bed for SiC and ZrO_2 at different energy flux densities. "Exp" refers to experimental results of (Flamant, 1982).

4.2. Model performance

In order to illustrate the usefulness of the proposed model a silicon carbide fluidized bed receiver with *ID* = 0.6 m is simulated. The effects of the operating conditions, such as the bed height, relative gas velocity and inlet air temperature on the receiver performance are studied. The receiver performance is calculated following Eq. 8. An energy flux of $\phi_{in} = 35 \cdot 10^4\ W/m^2$ is used in the following sections as it shows a good match between simulation and experimental results, Fig. 5.

Before starting the discussion of the results, Figure 6 illustrates the temperature profiles characterizing the two phases considered in the model for U_r = 3, *H/D* = 0.75 and $\phi_{in} = 35 \cdot 10^4\ W/m^2$. Due to the division of the airflow assumed by the two-phase model, the gas and solids in the emulsion phase reach the equilibrium temperature ($T_{s,e}$ and $T_{g,e}$ in Fig. 6). In contrast, the temperature of both the bubble voids and the through flow component is considerably lower than the temperature characterizing the emulsion phase (T_b in Fig. 6). This is caused by the bypass of fluidization gas through the visible bubble flow phase. As a result of having such division of the air flow, the air temperature at the outlet is obtained from the energy balance considering the air through the emulsion phase and through the visible bubble flow ($T_{g,out}$ in Fig. 6).

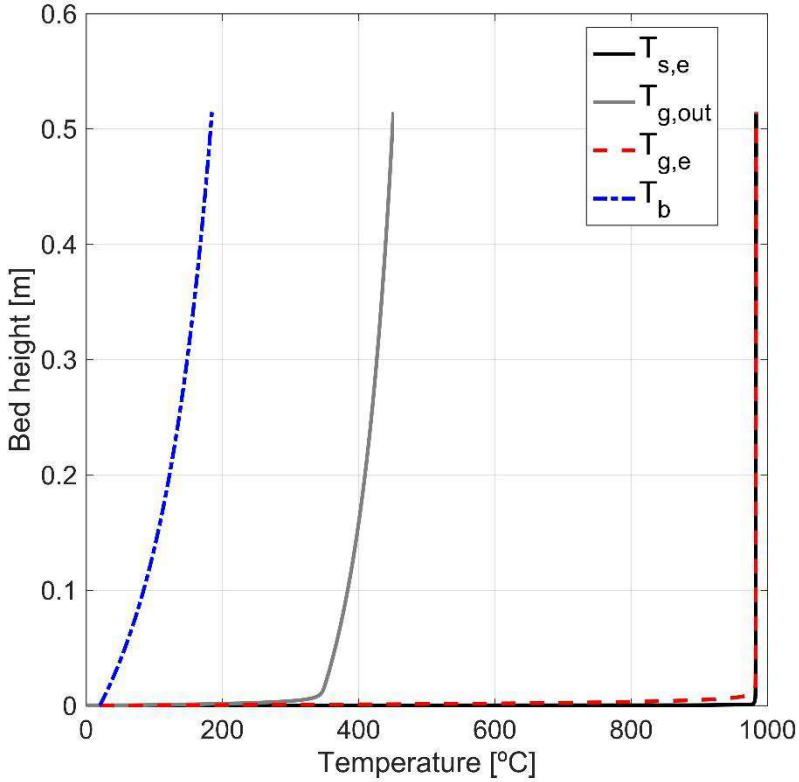

Figure 6. Temperature profiles model output: solid phase and interstitial gas temperature at the emulsion phase (black solid and red dotted lines), visible bubble flow temperature (blue dotted line), outlet air temperature (grey solid line).

4.2.1. Bed height effect

The influence of the static bed height, *H/D*, is analyzed considering different bed aspect ratios for constant operating conditions of $\phi_{in} = 35 \cdot 10^4\ W/m^2$ and $T_{air,in}$ = 20ºC. In order to choose the bed height, it is critical to establish a compromise between fluidization quality (bubbling regime) and degree of mixing (bubble size). A value of U_r = 2 is typically employed to ensure good fluidization conditions when operating in the bubbling regime with shallow bed configurations in a range of 0.5 < *H/D* < 1. Complete bed fluidization is guaranteed at these conditions while slugging is avoided (Kunii and Levenspiel, 1991). However, as described below (Fig. 8), a

slightly higher value of U_r = 3 is used because it facilitates working near a local maximum of the thermal solids efficiency.

Figure 7 shows that the bed aspect ratios ranging between 0.5 < *H*/*D* < 1 at U_r = 3 have little effect on both the bed and outlet gas temperatures, showing a variation of the gas efficiency less than 2%. As the bed height shows a reduced influence on the receiver temperatures, the following results will be obtained considering a bed with an aspect ratio of *H/D* = 0.75. Such bed aspect ratio means a bed height of 0.45 m, which involves a bed at shallow bed operation conditions characterized by good mixing properties.

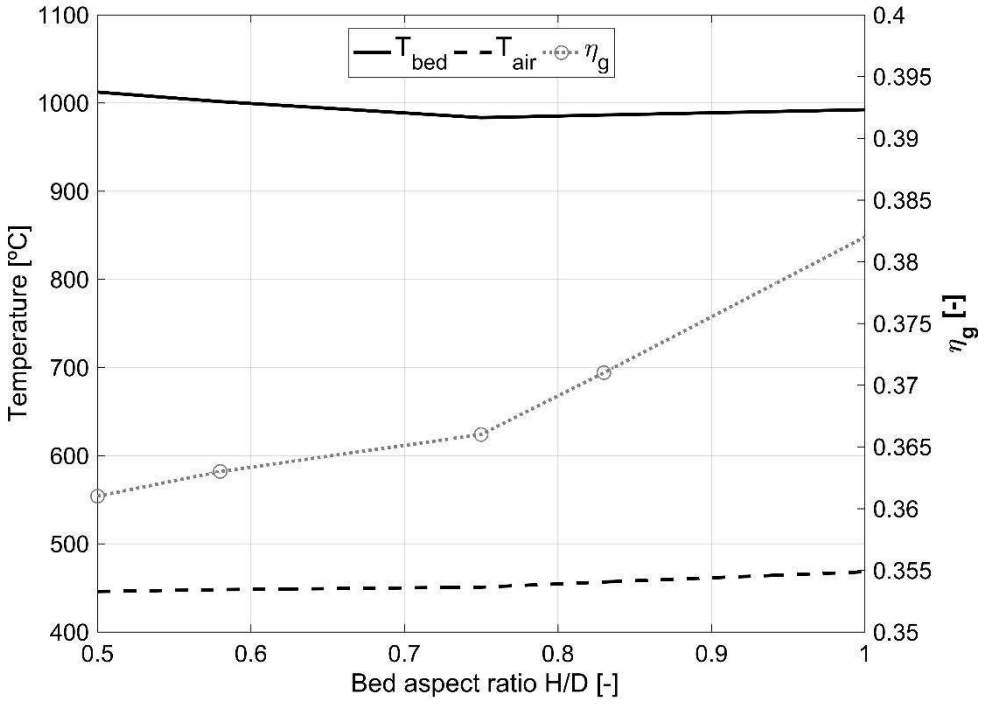

Figure 7. Bed height effect on the receiver temperatures and gas efficiency at steady state (U_r = 3, ϕ_{in} = 35·10^4 W/m^2, $T_{air,in}$ = 20ºC).

4.2.2. Relative gas velocity effect

The superficial gas velocity, U_0, is directly related to the fluidization regime that characterizes the fluidized bed dynamics, changing from poor to vigorous fluidization conditions with an increase of this parameter (Zijerveld et al., 1998). Accordingly, it can be generally stated that the gas solid mixing increases as the superficial gas velocity increases. However, the increase of the superficial gas velocity rises the energy cost associated with air blowers. As stated above, the fluidized bed particle receiver will be operated in bubbling conditions due to their advantageous properties of heat and mass transfer. Thus, the bed should operate at low relative gas velocities well below turbulent regime conditions to decrease the parasitic consumptions, but at high enough values to provide good fluidization properties to ensure good heat and mass transfer coefficients. A bed with of *H/D* = 0.75 and ϕ_{in} = 35·10^4 W/m^2 is simulated following the results of Fig. 7.

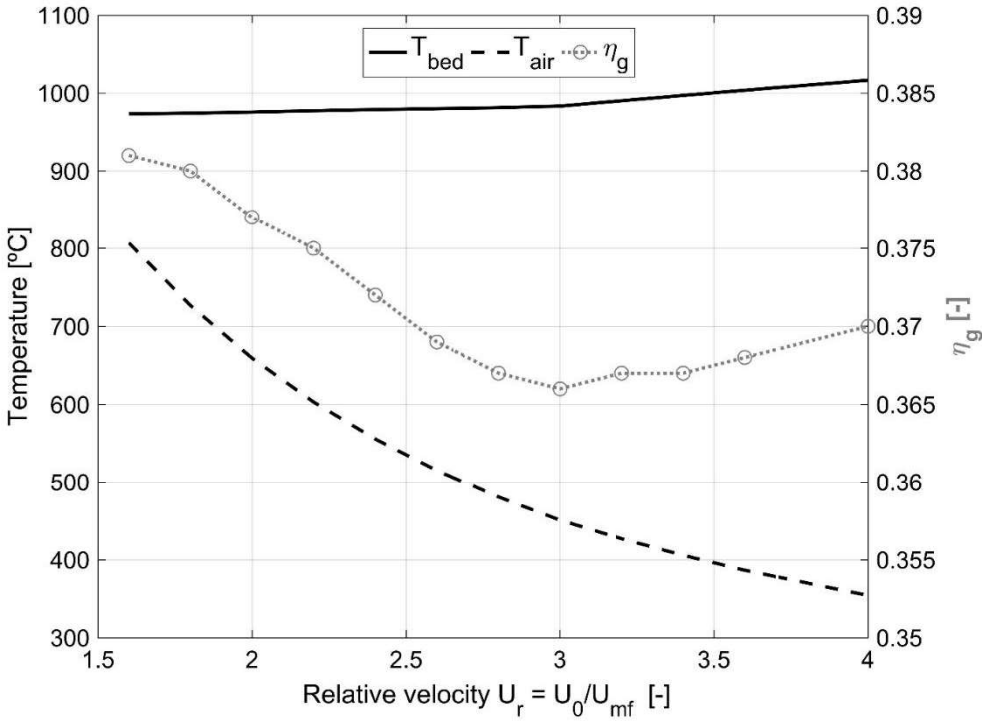

Figure 8. Relative superficial gas velocity effect on gas thermal efficiency and exit gas and bed stationary-state temperatures (H = 0.45 m, ϕ_{in} = 35·10^4 W/m^2, $T_{air,in}$ = 20ºC).

Figure 8 analyzes particle and gas temperatures, on the left axis, and the gas efficiency on the right axis, for several relative velocities. Figure 8 shows that the gas temperature is reduced when increasing the fraction of gas that leaves the bed. Consequently, as the energy losses from the particles have been reduced, the particles temperature increases. The gas efficiency decreases up to U_r =3. Later, higher gas velocities result in an improvement of the mixing properties, and consequently, the gas efficiency increases. Therefore, a value of U_r =3 is selected in order to minimize the gas losses while reducing the parasitic consumption caused by the airflow.

4.2.4. Inlet air temperature effect

Inlet air temperature is a key operating condition for any heat transfer process in fluidized beds. Its influence is studied for the conditions set before: U_r = 3, H/D = 0.75 and $\emptyset_{in}$ = 35·10^4 W/m^2. Figure 9 shows how, as the inlet air temperature increases, the energy losses from the particle to the gas decrease due to the lower temperature difference between gas and particles. Therefore, the gas thermal efficiency, which is measured as the heat gained by the air, decreases when increasing the temperature of the inlet air. It is worth to mention that a temperature rise of approximately 300 ºC of the inlet gas, leads to a solids temperature rise of about 90ºC, pointing out that the stationary bed temperature is mainly driven by the incoming heat flux rather than from convection losses to the gas side for the high heat fluxes covered in this research.

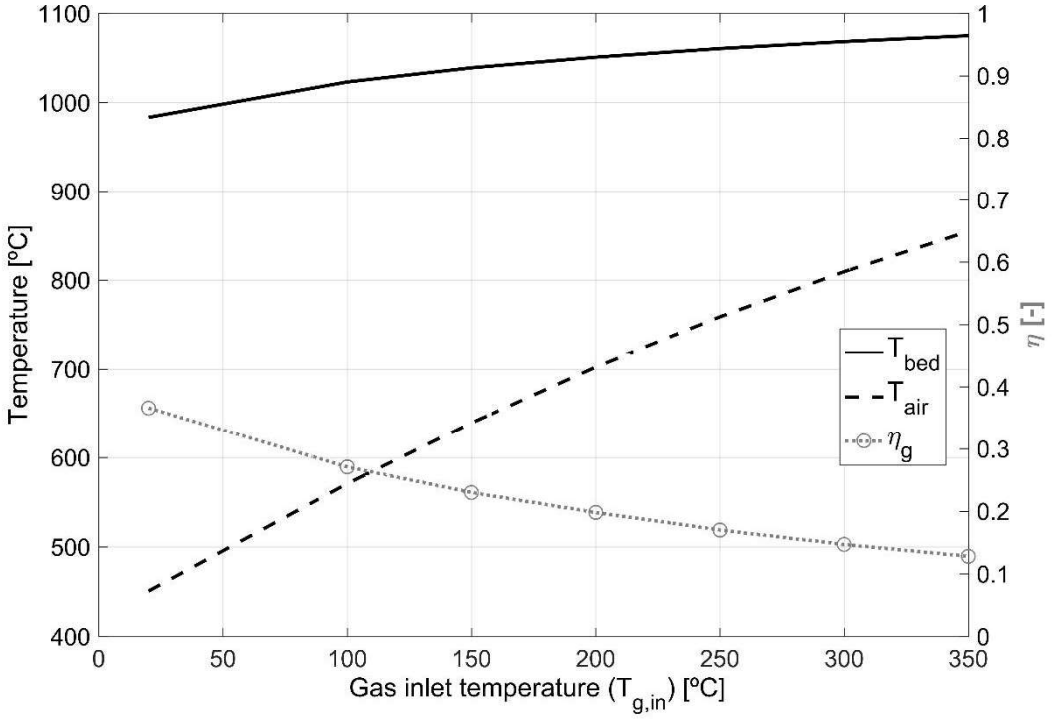

Figure 9. Inlet air temperature effect on the efficiency and stationary-state temperatures of both gas and particles (U_r = 3, *H/D* = 0.75 and ϕ_{in} = 35·10^4 W/m^2).

4.3. Open loop time response

Prior to building a beam-down fluidized bed receiver, it is critical to know the characteristic times of each zone needed to reach steady state conditions. Due the large value of the heat flux energies that characterize beam-down particle receiver and the good properties of gas-solid fluidized beds, a fast temporal response of these systems can be anticipated. In order to give a measure of how fast that response could be, Figure 10 shows the time-reaction curves provided by the model for zones 1, 2 and 3. The size of the different zones has been set to be 1/3 of the actual bed height.

Figure 10 shows that, although the time reaction curves behave as 2nd order underdamped system, the different zones can be roughly approximated as a first order system and then an open loop time constant can be used to measure the dynamical response of the receiver. According to that, the open loop time constant is computed as the time (τ) in which the bulk bed temperatures reach 0.623 times the value of the steady state value. Thus, τ_1 = 14.9 s; τ_2 = 33.8 s, τ_3 = 49 s. These conservative times can be used estimate the time needed to reach the stationary state of bulk temperature at the operational conditions shown in Fig. 9, which would be around 4τ_3 = 196 s. Such value reveals that the fluidized bed particle beam down receptor is characterized by short reaction times when properly operated.

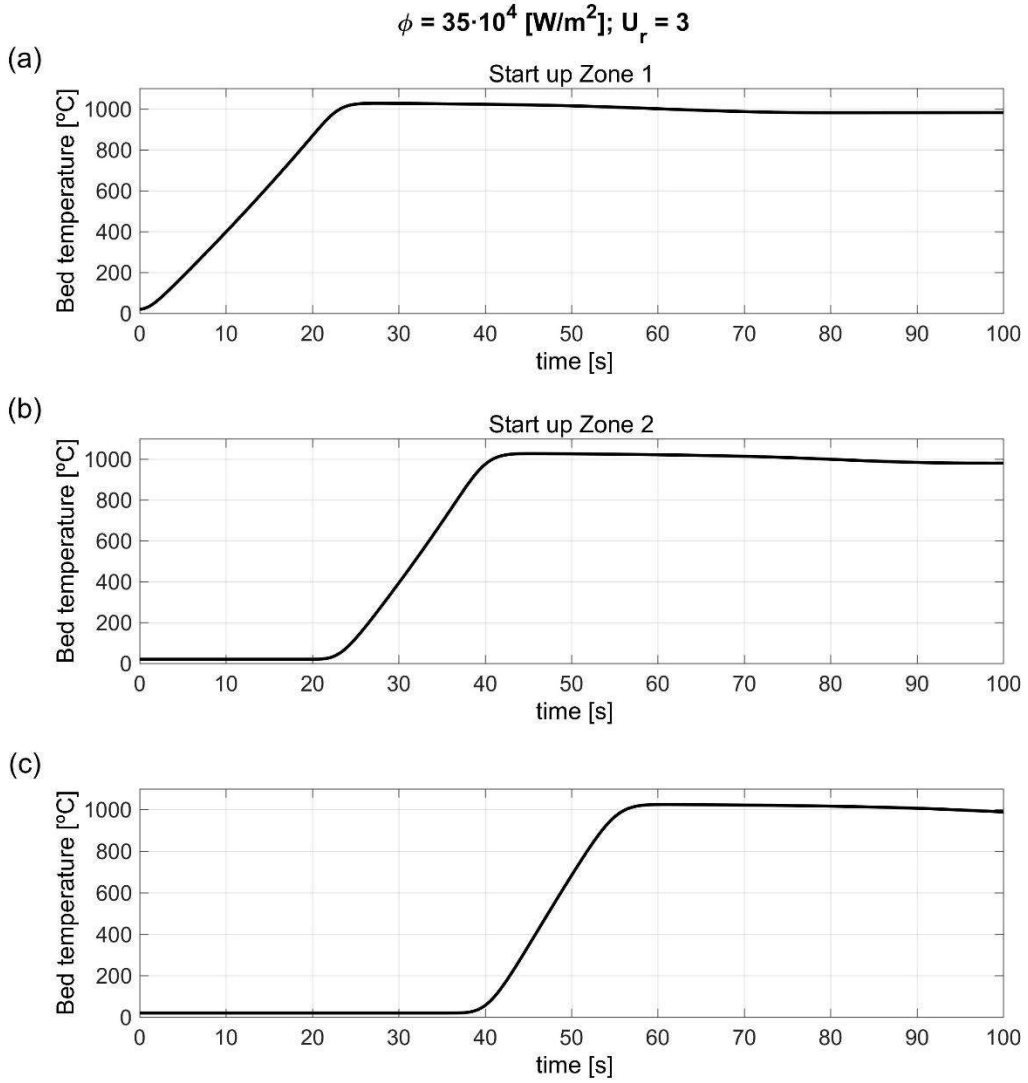

Figure 10. Time reaction curves for H = 0.45 m, U_r = 3, $\emptyset_{in}$= 35·10^{4}W/m^2 and $T_{air,in}$ = 20ºC: a) Zone 1 (surface region); b) Zone 2 (middle region); c) Zone 3 (bottom region).

Figure 11 shows the bed temperature profiles for different times. The temperature evolution during this transient response shows how the energy captured in the top of the bed is transferred to the bed bottom. The final temperature profile characterizing the steady-state bulk temperature distribution in the bed is shown in black solid line after t = 125 s, Fig. 11. It is clear that, at the operational conditions used during the transient simulation, the bed is very well mixed without temperature gradients once the stationary state is achieved.

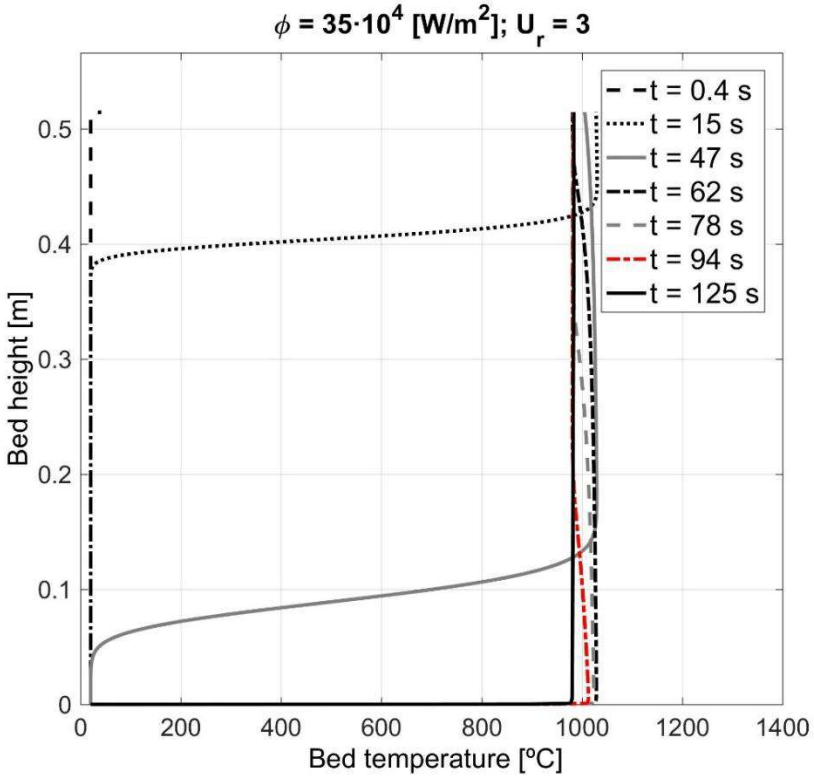

Figure 11. Bed temperatures profiles for different times during the start-up process (H = 0.45 m, U_r = 3, $\emptyset_{in}$ = 35·10^4 W/m^2 and $T_{air,in}$ = 20ºC).

5. Conclusions

The new two-phase model proposed in this paper describes the vertical temperature distribution in a fluidized bed directly irradiated from the top. The model describes phenomenologically the heat transfer processes within a bubbling gas-solid fluidized bed, enhancing the relevance of the solid convection mechanism and showing the influence of the operating conditions on the receiver performance. Thus, the model can be used as a powerful design tool for thermochemical or energy capture applications.

The model has been validated against experimental results of the literature simulating beds operated with silicon carbide and zirconia particles. An increase of the bulk bed and air exit temperatures is observed as the heat flux increases. A close match between the model and previously reported data is shown for silicon carbide particles tests. Zone 2, which corresponds to the central part of the fluidized bed system, and zone 3, which corresponds to the bottom region, have been identified. In the case of the zirconia particles, the model deviates from the reported data. Therefore, particle properties are a critical aspect to model fluidized beds operating at high temperature conditions.

The proposed model identifies the solid convection as the dominant heat transfer mechanism in fluidized bed beam down receivers. In order to achieve an adequate solid circulation process, the selection of proper bed height and superficial gas velocity becomes critical. In this line, it has been shown the low influence of the bed aspect ratio on the bed and air temperatures. For the case study considered using SiC as particulate material, a relative superficial gas velocity of U_r = 3 ensures a good mixing degree to provide an adequate fluidization state and good gas-solid mixing for H/D = 0.75. As expected from the good heat and mass transfer properties of gas-solid

fluidized beds, the particle beam down receptor is characterized by short reaction rates when properly operated, which benefit the potential industrial uses of the receptor.

The thick approximation, which follows the diffusion approach, used to solve the problem of radiation heat transfer within the bed emulsion explains the radiation phenomena along the receptor. Moreover, it has been observed that the extinction coefficient values provided by this approach present the same order of magnitude than the extinction coefficient reported previously in the literature.

Nomenclature

Abbreviations

CSP concentrating solar power

CFD computational fluid dynamics

DEM discrete element method

Symbols

a_B bubbles fraction (-)

a_{BW} bubbles and wakes fraction (-)

a_p specific surface of particles (m^{-1})

A_{bed} bed surface (m^2)

$A_{p,sL}$ effective heat transfer area of all particles at the top layer surface (m^2)

c_p specific heat (J/kg/K)

d_p sieve particle diameter (µm)

d_B bubble diameter (m)

D bed diameter (m)

f_w wake volume fraction (-)

f_v particle volume fraction (-)

F_{b-a} vision factor (-)

F_{ij} coaxial parallel disk vision factor (-)

g gravity (m/s^2)

H settle bed height (m)

ID internal diameter (m)

h_{gp} particle to gas heat transfer coefficient (W/m^2K)

h_{bc} bubble gas to dense bed heat transfer coefficient (W/m^2K)

k_e effective thermal conductivity (W/mK)

k_e^0 effective thermal conductivity of a fixed bed with a stagnant gas (W/mK)

k_g thermal conductivity of gas (W/mK)

k_r radiative conductivity (W/mK)

k_s particle conductivity (W/mK)

$\dot{m}$ mass flow (kg/s)

n refractive index (-)

q_r radiative heat flux (W/m^2)

Q_a absorption scatter property (-)

Q'''_{sc} heat transferred by the solid circulation (W/m^3)

Q'''_{gs} heat gained by emulsion gas (W/m^3)

Q'''_{bbs} heat gained by bubbles (W/m^3)

Re_p rarticle Reynolds number (-)

t time (s)

T temperature (K)

T_{sky} effective temperature for radiative heat losses (K)

U gas velocity (m/s)

U_0 superficial gas velocity (m/s)

U_{mf} minimum fluidization velocity (m/s)

U_r relative superficial gas velocity (-)

w circulation rate based on bulk phase (m/s)

z bed height (m)

Greek symbols

α_{bed} effective isothermal bed absorptivity (-)

β_R mean extinction coefficient (m^{-1})

ΔP_{dist} distributor pressure drop (Pa)

ΔP_{bed} bed pressure drop (Pa)

ε_{eff} effective bed surface emissivity (-)

ε_p particle emissivity (-)

ε_0 void fraction (-)

ε_e emulsion void fraction (-)

η_g receiver gas thermal efficiency (-)

ρ density (kg/m^3)

σ Stephan-Boltzman constant (W/m^{2}K^4)

τ open loop time constant (s)

$\emptyset_{in,a_p}$ total energy flux absorbed at the bed surface per surface of particles (W/$m^2_{A_{p,sL}}$)

$\emptyset_{in}$ energy flux received at the bed surface per bed surface (W/m^2)

Subscripts

amb ambient

b bubble

e emulsion

g gas

s solid

APPENDIX

A. View factor relations (Modest, 2013)

i. Differential planar element to sphere – normal to center of element passes through center of sphere:

$$F_{b-a} = \left(\frac{r}{h}\right)^2 \quad \text{A.1}$$

ii. Differential planar element to sphere – tangent to element passes through center of sphere:

$$F_{b-a} = \frac{1}{h}\left[tan^{-1}\frac{1}{\sqrt{\left(\frac{h}{r}\right)^2-1}} - \frac{\sqrt{\left(\frac{h}{r}\right)^2-1}}{\left(\frac{h}{r}\right)^2}\right] \quad \text{A.2}$$

Acknowledgments

This work has been supported by the Spanish Government under the project ENE2015-69486-R (MINECO/FEDER, UE)

References

Alovisio, A., Chacartegui, R., Ortiz, C., Valverde, J.M., Verda, V., 2017. Optimizing the CSP-Calcium Looping integration for Thermochemical Energy Storage. Energy Convers. Manage. 136, 85-98.

Bell, I.H., Wronski, J., Quoilin, S., Lemort, V., 2014. Pure and pseudo-pure fluid thermophysical property evaluation and the open-source thermophysical property library coolprop. Ind Eng Chem Res 53, 2498-2508.

Bellan, S., Matsubara, K., Cho, H.S., Gokon, N., Kodama, T., 2018. A CFD-DEM study of hydrodynamics with heat transfer in a gas-solid fluidized bed reactor for solar thermal applications. Int. J. Heat Mass Transf. 116, 377-392.

Bokkers, G.A., Laverman, J.A., Annaland, M.v.S., Kuipers, J.A.M., 2006. Modelling of large-scale dense gas-solid bubbling fluidised beds using a novel discrete bubble model. Chemical Engineering Science 61, 5590-5602.

Briongos, J.V., Aragon, J.A., Palancar, M.C., 2007. Phase space structure and multi-resolution analysis of gas-solid fluidized bed hydrodynamics: Part II: Dynamic analysis. Chemical Engineering Science 62, 2865-2879.

Briongos, J.V., Sobrino, C., Gómez-Hernández, J., Santana, D., 2013. Characterization of flow-induced vibrations in gas-solid fluidized beds: Elements of the theory. Chemical Engineering Science 93, 181-196.

Calvet, N., Martins, M., Grange, B., Perez, V.G., Belasri, D., Ali, M.T., Armstrong, P.R., 2016. The Masdar Institute solar platform: A new research facility in the UAE for development of CSP components and thermal energy storage systems. AIP Conf. Proc. 1734.

Chen, J.C., Chen, K.L., 1981. Analysis of simultaneous radiative and conductive heat transfer in fluidized beds. Chem. Eng. Commun. 9, 255-271.

Chen, J.C., Grace, J.R., Golriz, M.R., 2005. Heat transfer in fluidized beds: Design methods. Powder Technol 150, 123-132.

Darton, R.C., LaNauze, R.D., Davidson, J.F., Harrison, D., 1977. BUBBLE GROWTH DUE TO COALESCENCE IN FLUIDISED BEDS. Trans Inst Chem Eng 55, 274-280.

Davidson, J.F., Clift, R., Harrison, D., 1985. Fluidization, 2 ed. Academis Press Inc., Orlando, Florida 32887.

Davidson, J.F., Harrison, D., 1963. Fluidised Particles, 1st ed. Cambridge University Press, Great Britain.

Daw, C.S., Lawkins, W.F., Downing, D.J., Clapp, N.E., 1990. Chaotic Characteristics of a Complex Gas-Solids Flow. Physical Review a 41, 1179-1181.

Flamant, G., 1982. Theoretical and experimental study of radiant heat transfer in a solar fluidized-bed receiver. AIChE J. 28, 529-535.

Flamant, G., Lu, J.D., Variot, B., 1992. Radiation heat transfer in fluidized beds: a comparison of theoretical approaches. ASME Heat Transfer Div Publ HTD 203, 215-220.

Flamant, G., Olalde, G., 1983. High temperature solar gas heating comparison between packed and fluidized bed receivers-I. Sol. Energy 31, 463-471.

Gao, W.M., Kong, L.X., Hodgson, P.D., 2002. Numerical simulation of heat and mass transfer in fluidised bed heat treatment furnaces. J. Mater. Process. Technol. 125-126, 170-178.

Geldart, D., 1986. Gas Fluidization Technology. John Wiley & Sons Ltd., Great Britain.

Geldart, D., 1973. Types of gas fluidization. Powder Technol 7, 285-292.

Geldart, D., Abrahamsen, A.R., 1978. Homogeneous fluidization of fine powders using various gases and pressures. Powder Technol 19, 133-136.

Gokon, N., Ono, R., Hatamachi, T., Liuyun, L., Kim, H.-., Kodama, T., 2012. CO2gasification of coal cokes using internally circulating fluidized bed reactor by concentrated Xe-light irradiation for solar gasification. Int J Hydrogen Energy 37, 12128-12137.

Gómez-Hernández, J., González-Gómez, P.A., Ni-Song, T., Briongos, J.V., Santana, D., Santiago de Chile, Chile, 2017. Design of a Solar Linear Particle Receiver Placed at the Ground Level. Conference Paper, Solar Power & Chemical Energy Systems (SolarPACES) , 26-29.

Grace, J.R., Clift, R., 1974. On the two-phase theory of fluidization. Chem. Eng. Sci. 29, 327-334.

Ho, C.K., 2016. A review of high-temperature particle receivers for concentrating solar power. Appl. Therm. Eng. 109, 958-969.

Incropera, F.P., Dewitt, D.P., Bergman, T.L., Lavine, A.S., 2013. Principles of Heat and Mass Transfer, 7 Ed. ed. John Wiley & Sons, Singapore.

Johnsson, F., Zijerveld, R., Schouten, J., van den Bleek, C., Leckner, B., 2000. Characterization of fluidization regimes by time-series analysis of pressure fluctuations. Int. J. Multiphase Flow 26, 663-715.

Knowlton, T.M., 1999. 2 - Pressure and Temperature Effects in Fluid-Particle Systems, in Yang, W. (Ed.), Fluidization, Solids Handling, and Processing. William Andrew Publishing, Westwood, NJ, pp. 111-152.

Kodama, T., Gokon, N., Cho, H.S., Matsubara, K., Kaneko, H., Senuma, K., Itoh, S., Yokota, S.-., 2017. Particles fluidized bed receiver/reactor tests with quartz sand particles using a 100-kWthbeam-down solar concentrating system at Miyazaki. AIP Conf. Proc. 1850.

Kodama, T., Gokon, N., Enomoto, S.-., Itoh, S., Hatamachi, T., 2010. Coal coke gasification in a windowed solar chemical reactor for beam-down optics. J Sol Energy Eng Trans ASME 132.

Kodama, T., Gokon, N., Matsubara, K., Yoshida, K., Koikari, S., Nagase, Y., Nakamura, K., 2013. Flux measurement of a new beam-down solar concentrating system in Miyazaki for demonstration of thermochemical water splitting reactors. Energy Procedia 49, 1990-1998.

Kunii, D., Levenspiel, O., 1991. Fluidization Engineering, 2nd ed. Butterworth-Heinemann, USA.

Lockett, M.J., Davidson, J.F., Harrison, D., 1967. On the two-phase theory of fluidisation. Chem. Eng. Sci. 22, 1059-1066.

Mazza, G.D., Berto, C.A., Baffeto, G.F., 1991. Evaluation of radiative heat transfer properties in dense particulate media. Powder Technol 67, 137-144.

Modest, M.F., 2013. Radiative Heat Transfer, 3rd ed. Academic Press, Burlington.

Molerus, O., 1997a. Heat Transfer in Fluidized Beds, 1st ed. Chapman and Hall, London.

Molerus, O., 1997b. Heat Transfer in Fluidized Beds, 1st ed. Chapman and Hall, Londres.

Molerus, O., 1982. Interpretation of Geldart's type A, B, C, and D powders by taking into account interparticle cohesion forces. Powder Technol 33.

Mori, S., Wen, C.Y., 1975. Estimation of bubble diameter in gaseous fluidized beds. AIChE J. 21, 109-115.

Mullinger, P., Jenkins, B., 2008. Chapter 4 - An introduction to heat transfer in furnaces, in Mullinger, P., Jenkins, B. (Eds.), Industrial and Process Furnaces. Butterworth-Heinemann, Oxford, pp. 89-140.

Ortiz, C., Chacartegui, R., Valverde, J.M., Alovisio, A., Becerra, J.A., 2017. Power cycles integration in concentrated solar power plants with energy storage based on calcium looping. Energy Convers. Manage. 149, 815-829.

Segal, A., Epstein, M., 2003. Solar ground reformer. Sol. Energy 75, 479-490.

Segal, A., Epstein, M., 2000. The optics of the solar tower reflector. Sol. Energy 69, 229-241.

Segal, A., Epstein, M., 1997. Modeling of solar receiver for cracking of liquid petroleum gas. J Sol Energy Eng Trans ASME 119, 48-51.

Shabanian, J., Chaouki, J., 2017. Effects of temperature, pressure, and interparticle forces on the hydrodynamics of a gas-solid fluidized bed. Chemical Engineering Journal 313, 580-590.

Siegel, N., Gross, M., Ho, C., Phan, T., Yuan, J., 2013. Physical properties of solid particle thermal energy storage media for concentrating solar power applications. Energy Procedia 49, 1015-1023.

Strieder, W., 1997. Radiation heat transport in disordered media. Adv. Water Resour. 20, 171-187.

Tien, C.L., 1988. Thermal radiation in packed and fluidized beds. J. Heat Transf. 110, 1230-1243.

Tregambi, C., Chirone, R., Montagnaro, F., Salatino, P., Solimene, R., 2016. Heat transfer in directly irradiated fluidized beds. Sol. Energy 129, 85-100.

Tregambi, C., Montagnaro, F., Salatino, P., Solimene, R., 2017. Directly irradiated fluidized bed reactors for thermochemical processing and energy storage: Application to calcium looping. AIP Conf. Proc. 1850.

Van Wachem, B.G.M., Schouten, J.C., Van den Bleek, C.M., Krishna, R., Sinclair, J.L., 2001. Comparative analysis of CFD models of dense gas-solid systems. AIChE J. 47, 1035-1051.

Vant-Hull, L., 2013. Issues with beam-down concepts. Energy Procedia 49, 257-264.

Verein, D.I., 2010. VDI Heat Atlas. Springer Berlin Heidelberg, Berlin, Heidelberg, Berlin, Heidelberg.

Yadav, D., Banerjee, R., 2016. A review of solar thermochemical processes. Renewable Sustainable Energy Rev 54, 497-532.

Yates, J.G., 1996. Effects of temperature and pressure on gas-solid fluidization. Chemical Engineering Science 51, 167-205.

Zijerveld, R.C., Johnsson, F., Marzocchella, A., Schouten, J.C., van den Bleek, C.M., 1998. Fluidization regimes and transitions from fixed bed to dilute transport flow. Powder Technol 95, 185-204.